J. Fluid Mech. (1976), *vol.* 78, *part* 3, *pp.* 489–512
Printed in Great Britain

Selective withdrawal from a finite rectangular tank

By JORG IMBERGER, RORY THOMPSON†
Department of Mathematics, The University of Western Australia, Nedlands, Western Australia 6009

AND CHRIS FANDRY
Department of Mathematics, Monash University, Clayton, Victoria 3168, Australia

(Received 7 July 1975)

The time development of two-dimensional fluid motion induced by a line sink in a rectangular, density stratified reservoir with a free surface is given. It is shown that the initiation of such a sink gives birth to a spectrum of internal expanding shear fronts with a progressively decreasing vertical wavelength. These fronts move out from the sink and travel towards the far wall, where they are reflected. This process ceases once the front with a vertical wavelength equal to the steady withdrawal-layer thickness has reached the end wall. The fronts so introduced continue to move back and forth, expanding to standing waves if the viscosity of the fluid is small enough. The evolution and nature of the withdrawal layer are shown to depend critically on the relative magnitude of the convective inertia and viscous forces, the number of reflexions from the rear wall and the Prandtl number.

1. Introduction

Recently there has been a renewed interest in the problem of two-dimensional selective withdrawal from a stratified reservoir. The papers by Pao & Kao (1974) and Imberger & Fandry (1975) have considerably advanced our understanding of both the mechanisms of the withdrawal-layer establishment and the effect of a vertical upstream boundary. These papers were both confined to viscously dominated withdrawal-layer formation, but even then they offered two, apparently different, models for the same process. The present study investigates withdrawal flow for the whole possible parameter range. The solutions found offer a reconciliation of the above two apparently different models.

Imberger (1972) assumed that in reservoirs with small depth-to-length ratios the upstream boundary is unimportant and may be replaced by a uniform flow supplying the fluid drained off at the sink. Using such a horizontal-duct model, Pao & Kao (1974) were able to show that a steady state was established by shear fronts travelling out from the sink against the induced uniform upstream velocity. These fronts were identical to those investigated by McEwan & Baines (1974), who showed that the speed of the nth wave was given by $HN/n\pi$, where

† Present address: Geofysisk Institutt, Universitetet i Bergen, Bergen, N5000, Norway.

$2H$ was the depth of the reservoir, N the Brunt–Väisälä frequency and n the mode number of the wave. Furthermore, as these modes propagated down the reservoir the flow collapsed into a withdrawal-layer structure until it had reached the asymptotic state described by Imberger (1972). The characteristic time necessary to establish a pseudo-steady state for a reservoir of length L was estimated to be $O(L/2HN)$, i.e. the time required for the first mode to reach the far end of the reservoir. In a companion paper, Kao, Pao & Wei (1974) experimentally supported their theoretical findings and presented conclusive evidence for the existence of such fronts, their speed of propagation and their rate of expansion. However, the experimental investigations were not carried out long enough to establish conclusively the time required for a steady state to be achieved over the whole length of their tank.

Imberger & Fandry (1975) noticed that a rear wall blocking the flow had a severe effect on the flow, especially once the first mode had reached the rear wall and a withdrawal layer had begun to form. Once this had occurred, the fluid below the partially formed layer had essentially stagnated and the fluid above the layer moved with a uniform vertical velocity, just sufficient to balance the fluid withdrawn. Thus they postulated that once a layer had begun to form the vertical extent of the fluid above and below the layer was unimportant. This hypothesis allowed the problem to be modelled by flow in a vertical duct. Their analysis explained the formation of a withdrawal layer, but the motion was composed of a continuous spectrum and not a discrete spectrum of simple progressive shear fronts. Their work was confined to fluids with a Pr number $O(1)$ and it showed that the time taken for a withdrawal layer of thickness $O(Ra^{-\frac{1}{3}}L)$ to form was $O(Ra^{\frac{1}{3}}N^{-1})$, provided $FRa^{\frac{1}{3}} < 1$. The Rayleigh number Ra was defined by $N^2L^4/\nu\kappa$ and the Froude number F was given by Q/NL^2, where Q was the discharge, L the duct width, N the Brunt–Väisälä frequency and ν and κ the kinematic viscosity and molecular diffusivity of the stratifying species respectively.

In the present investigation it is shown that the sudden initiation of a line sink in a finite reservoir with a free surface leads to the following sequence of events. Immediately after the sink is turned on a nearly horizontal potential flow is established in which the horizontal velocity decreases linearly to zero at the end of the tank. This flow is progressively modified by shear fronts which are continually attenuated by diffusion of vorticity and mass and modified by the convection induced by the previous waves, which may or may not have already been reflected from the end walls. The nature of this evolution depends critically on the value of the parameter $R = FGr^{\frac{1}{3}}$, where $Gr = N^2L^4/\nu^2$. If R is smaller than one, the waves will travel out until they have decayed. Once a wave has decayed, no waves of smaller wavelength can propagate past this point of decay and a withdrawal-layer structure remains, the thickness of which is exactly equal to the wavelength of the smallest wave able to propagate to that station. It will be shown that this leads to a layer thickness $O(LGr^{-\frac{1}{3}})$ at the end of the tank and the time to reach the end wall is $O(N^{-1}Gr^{\frac{1}{3}})$. For very large Prandtl numbers, where $Pr = \nu/\kappa$, it will be shown in § 5 that such a layer is unsteady and subsequently collapse occurs.

Time scale	Comments
	Flow establishment
N^{-1}	Time scale for internal waves.
$N^{-1}\lambda^{-1}$	Time taken for the 1st shear wave to reach end.
$N^{-1}\lambda^{-3}$	Time taken for 1st mode to expand to a standing wave.
	Approach to steady state
(*a*) $R < Pr^{-\frac{5}{6}}$	
$N^{-1}Gr^{\frac{1}{6}}$	Initial withdrawal-layer formation. Layer collapses owing to convection of *in situ* gradient. $\delta = O(LGr^{-\frac{1}{6}})$.
$N^{-1}Gr^{\frac{1}{6}}Pr^{\frac{2}{3}}$	Pseudo-steady-state withdrawal as described by §3. $\delta = O(LGr^{-\frac{1}{6}}Pr^{-\frac{1}{6}})$.
$N^{-1}Gr^{\frac{1}{6}}Pr^{-\frac{1}{6}}R^{-1}$	Further collapse due to self-induced convection.
(*b*) $Pr^{-\frac{5}{6}} < R < Pr^{-\frac{1}{3}}$	
$N^{-1}Gr^{\frac{1}{6}}$	Initial withdrawal formation. $\delta = O(LGr^{-\frac{1}{6}})$.
$N^{-1}Gr^{\frac{1}{6}}R^{-\frac{4}{5}}$	Self-induced convection accelerates collapse. $\delta = O(LGr^{-\frac{1}{6}}R^{\frac{1}{5}})$.
$N^{-1}Gr^{\frac{1}{6}}Pr^{\frac{2}{3}}$	Steady state, as described by Imberger (1972), is reached; viscosity dominates. $L/x_c > 1$.
(*c*) $Pr^{-\frac{1}{3}} < R < 1$	
$N^{-1}Gr^{\frac{1}{6}}$	Initial withdrawal formation. $\delta = O(LGr^{-\frac{1}{6}})$.
$N^{-1}Gr^{\frac{1}{6}}R^{-\frac{4}{5}}$	Self-induced convection accelerates collapse. $\delta = O(LGr^{-\frac{1}{6}}R^{\frac{1}{5}})$.
$N^{-1}F^{-\frac{1}{2}}R^{-\frac{3}{2}}$	Steady state, as described by Imberger (1972), is reached; inertia dominates. $L/x_c < 1$.
(*d*) $R > 1$	
$N^{-1}F^{-\frac{1}{2}}$	Inertia dominates and solution behaves as described in §3. $\delta = O(LF^{\frac{1}{2}})$.
	Large times
$N^{-1}\lambda^2 Gr^{\frac{1}{2}}$	Time taken for all wave motion to decay.
LHQ^{-1}	Time taken for tank to empty.

TABLE 1. The hierachy of time scales. δ is the characteristic scale of the withdrawal-layer thickness. $N^{-1}Gr^{\frac{1}{6}}$ is the time taken for a viscous–buoyancy layer to form, or the time taken for waves of wavelength smaller than $LGr^{-\frac{1}{6}}$ to decay, or the time taken for mode $n = \lambda Gr^{\frac{1}{6}}$ to reach the end of the tank. $N^{-1}Gr^{\frac{1}{6}}R$ is the time taken for the inertial zone to be set up. $N^{-1}F^{-\frac{1}{2}}$ is the time needed for steady state to be achieved, or the time for wave $n = \lambda F^{-\frac{1}{2}}$ to reach the end of the tank, or the time for fluid to fall through a distance $LF^{\frac{1}{2}}$.

On the other hand, if R is larger than one, then convection dominates and waves will propagate out until the induced flow just balances their phase velocity. This occurs in time $O(N^{-1}F^{-\frac{1}{2}})$, which is the time required for a wave of wavelength equal to the withdrawal-layer thickness $O(LF^{\frac{1}{2}})$ to reach the end wall. Smaller waves are swept back out of the sink. In both cases this process may require many traverses by the leading shear front between the sink and the end wall and in this time it may expand to the full length of the tank to form a standing wave system before it is dissipated by viscosity or channelled into the withdrawal layer by convection. The hierachy of time scales is shown in table 1, where λ is the aspect ratio H/L.

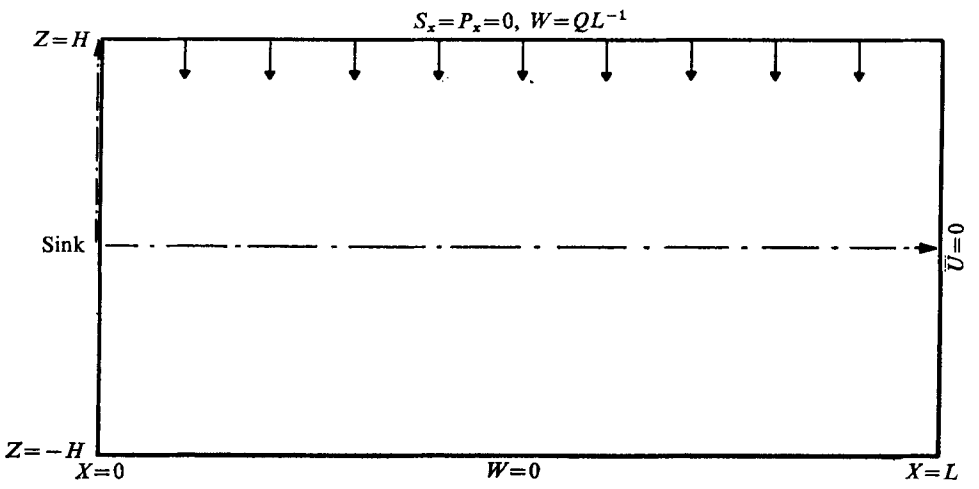

FIGURE 1. The geometry of the rectangular two-dimensional reservoir filled with linearly stratified fluid. The bottom and side walls are rigid, but slippery. The free surface is rigid and slippery, but descending at rate Q/L, where Q is the strength of the sink and L is the length of the reservoir. The total depth is $2H$.

2. Evolution of shear fronts into a withdrawal layer

Consider a rectangular container filled with a linearly stratified fluid which is being withdrawn through a line sink situated at the origin of the co-ordinate axes X, Z. Figure 1 shows the geometric configuration and the boundary conditions to be applied. The fluid is assumed to be both viscous and diffusive, but in order to avoid unnecessary complications the fluid is allowed to slip along any solid wall. In this way an understanding can be gained of the sink-initiated motion without the difficulty of wall boundary-layer formation. Provided the discharge Q is smaller than $L^{\frac{3}{2}}g^{\frac{1}{2}}$, the free-surface conditions, for times T small compared with HL/Q, will be given on $Z = H$ by

$$\Psi = [(X/L) - \tfrac{1}{2}]\,Q, \tag{1}$$

and

$$S = S_0 + S_0 H d\bar{S}/dZ + (QT/L)\,d\bar{S}/dZ, \tag{2}$$

where S_0 is the initial density at the level of the sink and $\bar{S}$ is the equilibrium density with no motion, assumed to be a linear function of Z.

In their experimental study, Kao, Pao & Wei (1974) found that immediately following the initiation of the sink a series of shear fronts propagated upstream against a nearly uniform horizontal potential flow. The time scale associated with these propagating fronts is N^{-1} and the vertical scale is H. McEwan & Baines (1974) in their study of analogous shear fronts have shown that the width of the primary shear front is $O(H(NT)^{\frac{1}{2}})$, and hence combining this with the above time scale yields a horizontal length scale H. The stream function ψ will be $O(Q)$, leading to vertical displacements $O(Q/HN)$, which in turn means that the density perturbations must be $O(H\lambda^{-2}Fd\bar{S}/dZ)$, where $\lambda = HL^{-1}$.

With these estimates the correct non-dimensional variables to introduce for the small-time initial flow regime are given by

$$x = XH^{-1}, \quad z = ZH^{-1}, \quad \psi = \Psi Q^{-1}, \quad s = S(d\bar{S}/dZ)^{-1}H^{-1}\lambda^2 F^{-1}, \quad t = TN.$$

In terms of these variables the Boussinesq approximation to the equations of motion is

$$\nabla^2\psi_t + \lambda^{-2}F(\psi_z\nabla^2\psi_x - \psi_x\nabla^2\psi_z) = s_x + (Pr/\lambda^4 Ra)^{\frac{1}{2}}(\nabla^2\psi_{zz} + \nabla^2\psi_{xx}), \tag{3}$$

$$s_t + \psi_x + \lambda^{-2}F(-\psi_x s_z + \psi_z s_x) = (Pr\lambda^4 Ra)^{-\frac{1}{2}}(s_{zz} + s_{xx}). \tag{4}$$

In the limit $F \to 0$ and $Ra \to \infty$ these equations can be reduced to the linear, inviscid, non-diffusive equation for the stream function ψ, i.e.

$$\nabla^2\psi_{tt} + \psi_{xx} = 0, \tag{5}$$

subject to the following boundary conditions for $t \geqslant 0$:

$$\text{(i) } \psi = \lambda x - \tfrac{1}{2} \text{ on } z = 1, \text{ (ii) } \psi = \tfrac{1}{2} \text{ on } z = 1, \text{ (iii) } \psi = -\tfrac{1}{2}\operatorname{sgn} z \text{ on } x = 0, \tag{6a–c}$$

$$\text{(iv) } \psi = \tfrac{1}{2} \text{ on } \lambda x = 1, \text{ (v) } (\partial/\partial t)\nabla^2\psi = 0, \nabla^2\psi = 0 \text{ at } t = 0. \tag{6d–f}$$

Although equation (5) is identical to that solved by Pao & Kao (1974) and McEwan & Baines (1974), the finite horizontal dimension leads to a different solution, for at least a certain range of time.

By taking the Laplace transforms of (5) and (6) it is easily shown that the solution for the transformed stream function $\bar{\psi}$ is given by

$$\bar{\psi}(x, z, s) = \tfrac{1}{2}s^{-1} + \tfrac{1}{2}s^{-1}(\lambda x - 1)(1 + z) + \sum_{n=1}^{\infty} \bar{a}_n(x, s)\sin n\pi z, \tag{7}$$

where
$$\bar{a}_n(x, s) = (n\pi s)^{-1}\sinh[\alpha(x - 1/\lambda)]/\sinh(\alpha/\lambda), \tag{8}$$

and
$$\alpha^2 = n^2\pi^2 s^2/(s^2 + 1). \tag{9}$$

Asymptotic inversion of (7) for very small times leads to

$$\psi(x, z, t) \sim \tfrac{1}{2} + \tfrac{1}{2}(\lambda x - 1)(1 + z) + \sum_{n=1}^{\infty} \frac{1}{n\pi} \frac{\sinh n\pi(x - 1/\lambda)}{\sinh(n\pi/\lambda)} \sin n\pi z, \tag{10}$$

which is just the potential flow solution showing a nearly linear decrease in horizontal velocity towards the end wall.

For times $0 < t < \pi/\lambda$, the inversion of (7) can be performed using the appropriate asymptotic representation of (8), which is

$$\bar{a}_n \sim (n\pi s)^{-1}\exp[-n\pi x s(s^2 + 1)^{-\frac{1}{2}}]. \tag{11}$$

As shown by Pao & Kao (1974) and McEwan & Baines (1974) this solution represents a discrete spectrum of shear fronts, propagating away from the sink upstream into the tank with constant non-dimensional speed $1/n\pi$, where n is the modal number of the nth front. Hence we can conclude that the finite-channel and infinite-horizontal-duct models display similar behaviour for times before the primary front is first reflected from the end wall. For times larger than π/λ^3,

which is the time taken for the primary front to expand to the length of the tank, a better representation is given by a sum of standing waves:

$$\psi(x,z,t) = \tfrac{1}{2}[\lambda x + (\lambda x - 1)\operatorname{sgn} z]\, H(t) + 2\pi^{-2} \sum_{n=1}^{\infty} \sum_{k=1}^{\infty} A_{nk} \sin k\pi\lambda x \cos(\omega_{nk} t) \sin n\pi z, \tag{12}$$

where $\omega_{nk} = (\lambda k/n)(1+\lambda^2 k^2/n^2)^{\frac{1}{2}}$, $A_{nk} = [\lambda nk(1+\lambda^2 k^2/n^2)]^{-1}$.

It is perhaps interesting to note that the infinite series in n is a slowly convergent one, but can be made to converge arbitrarily fast by an appropriate change in the boundary conditions at $x = 0$. If the boundary condition on ψ at $x = 0$ is replaced by

$$\psi(0,z,t) = \tfrac{1}{2}\{-\operatorname{erf}(z/a)/\operatorname{erf}(1/a)\} \exp(-b/4t), \tag{13}$$

then the amplitudes A_{nk} will be reduced by a factor

$$O(\exp[-\tfrac{1}{4}n^2\pi^2 a^2 - (\tfrac{1}{2}k\lambda b)^{\frac{1}{2}}(n^2 + k^2\lambda^2)^{-\frac{1}{4}}]). \tag{14}$$

Thus starting the sink slowly decreases the amplitude of the waves with a large horizontal wavenumber component (a much wider front will be observed initially) and introducing a distributed sink rather than a point sink reduces the amplitude of the waves with a large vertical wavenumber (and thus fewer shear wave modes will be observed). The limiting condition is achieved when b is $O(1)$ and a is $O(\lambda)$; then essentially no shear fronts or standing waves will be observed and the motion will be quasi-steady at all times and equal to the initial potential flow.

It is thus clearly seen that for long times the problem must be rescaled, as the solution (12) is non-uniform in both vertical distance and time. Two limiting cases may be distinguished depending on the magnitude of the parameter R. If R is small then the final withdrawal layer will be governed by a viscous–buoyancy force balance and if R is large then the balance will be between inertia and buoyancy.

3. The viscous–buoyancy withdrawal layer: $R \ll 1, Pr = O(1)$

As already stated in the introduction a withdrawal-layer structure will have formed when a wave is first dissipated at the end of the tank. For times of this magnitude the correct non-dimensional variables are

$$x' = XL^{-1}, \quad z' = ZL^{-1}Gr^{\frac{1}{6}}, \quad t' = TNGr^{-\frac{1}{6}}, \quad \psi' = \Psi Q^{-1},$$
$$s' = S(d\bar{S}/dZ)^{-1}L^{-1}R^{-1}Gr^{\frac{1}{6}}.$$

In terms of these new variables, but dropping the primes and eliminating the density, (3) and (4) may be written correct to $O(RPr^{\frac{5}{6}})$ and $O(Gr^{-\frac{2}{3}})$ as

$$Pr^{-1}\psi_{zzzzzz} - (1+Pr)/Pr\,\psi_{zzzzt} + \psi_{zztt} + \psi_{xx} + Gr^{-\frac{1}{3}}(\psi_{xxtt} + Pr^{-1}\psi_{zzzzxx} - (Pr+1)/Pr\,\psi_{xxzzt}) = 0. \tag{15}$$

By retaining the term $Gr^{-\frac{1}{3}}\psi_{xxtt}$, (15) contains all the terms of (5) and, as in Imberger & Fandry (1975), a uniformly valid solution for all time can be gen-

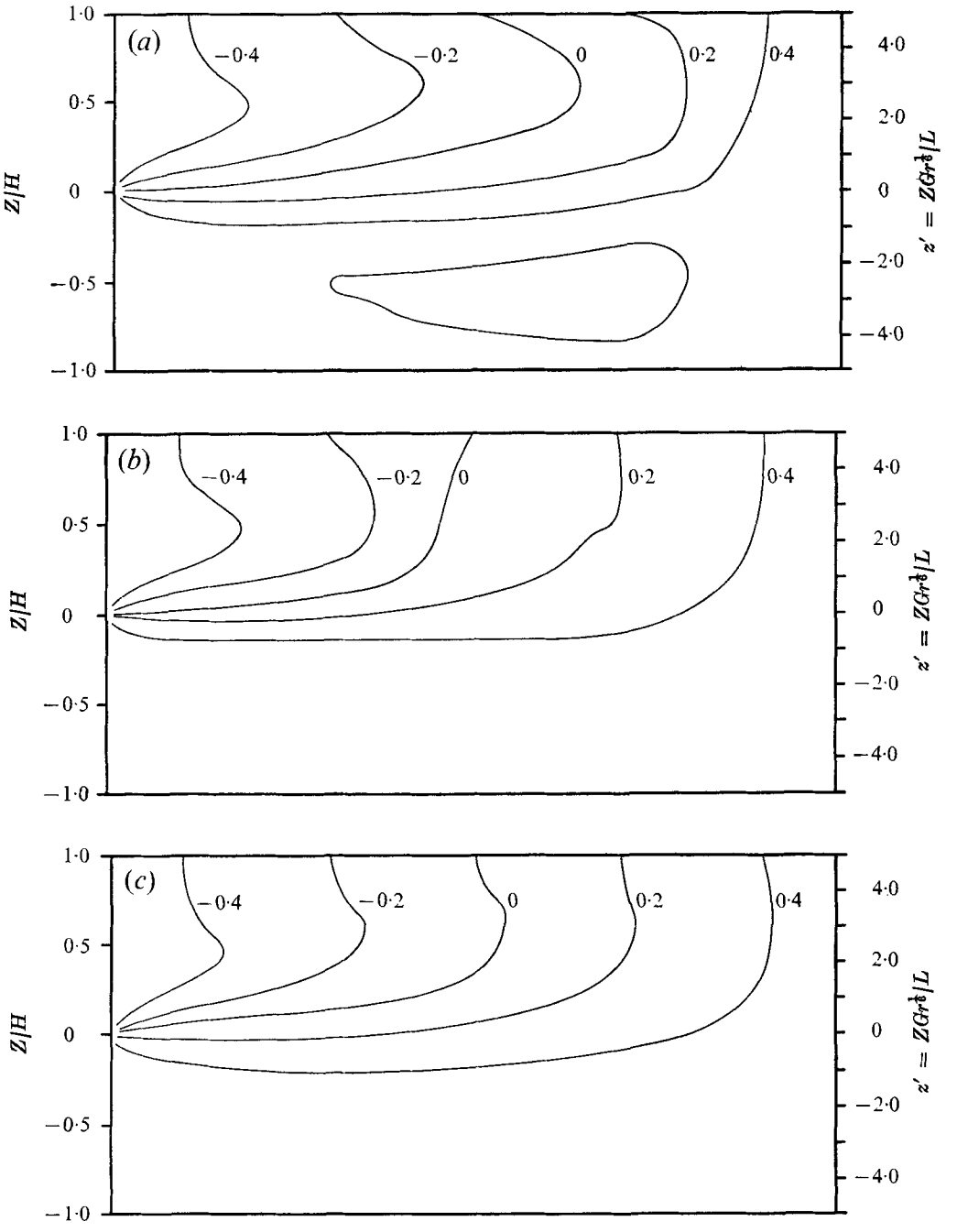

FIGURE 2. Streamlines for withdrawal from a stratified reservoir with $R < 1$ from (17). Parameters are $Pr = 1$, $\lambda = 0{\cdot}01$, $Gr = 4 \times 10^{15}$. (*a*) At non-dimensional time $t' = 0{\cdot}6$. Note the first shear wave at $x' = 0{\cdot}8$. (*b*) At non-dimensional time $t' = 1{\cdot}2$. The first wave has reflected to near $x' = 0{\cdot}4$; the second shear wave is visible near $x' = 0{\cdot}7$. (*c*) The steady solution (essentially valid for $t' > 2$). This is independent of Pr.

erated. However, as will become apparent below, it is more convenient to retain all the terms $O(Gr^{-\frac{1}{4}})$ even though some are negligibly small at all times. It will be assumed here that terms $O(RPr^{\frac{1}{2}})$ are small. A uniformly valid solution may thus be obtained by solving (15) subject to the following boundary conditions for $t \geqslant 0$. On

$$0 \leqslant x \leqslant 1 \quad \text{and} \quad \text{(i) } z = \beta\text{: } \psi = x - \tfrac{1}{2}, \quad \text{(ii) } z = -\beta\text{: } \psi = \tfrac{1}{2}. \tag{16a,b}$$

On $-\beta \leqslant Z \leqslant \beta$ and (iii) $x = 0$: $\psi = -\frac{1}{2}\operatorname{sgn} z$, (iv) $x = 1$: $\psi = \frac{1}{2}$, (16c, d)

where $\beta = \lambda Gr^{\frac{1}{4}}$. The solution is given by

$$\begin{aligned}\psi(x,z,t) = \tfrac{1}{2}[1+(x-1)(1+z/\beta)] + \sum_{n=1}^{\infty} \frac{1}{n\pi}\frac{\sinh\gamma(x-1)}{\sinh\gamma}\sin n\pi z/\beta \\ + \sum_{n=1}^{\infty}\sum_{k=1}^{\infty}(2/kn\pi^2 c)(1-b/d)\,e^{-\frac{1}{2}at}\{\cos[(d-\tfrac{1}{4}a^2)^{\frac{1}{2}}t] \\ + \tfrac{1}{2}a(d-\tfrac{1}{4}a^2)^{-\frac{1}{2}}\sin[(d-\tfrac{1}{4}a^2)^{\frac{1}{2}}t]\}\sin(n\pi z/\beta)\sin k\pi x,\end{aligned} \tag{17}$$

where

$$\gamma = b^{\frac{1}{2}}/[1+Gr^{-\frac{1}{4}}(n\pi/\beta)^4]^{\frac{1}{2}} \tag{18}$$

and

$$a = ((1+Pr)/Pr)(n\pi/\beta)^2, \quad c = 1+Gr^{-\frac{1}{4}}k^2\beta^2/n^2,$$
$$b = Pr^{-1}(n\pi/\beta)^4, \quad d = b + k^2\beta^2/n^2cPr. \tag{19}$$

Once again the solution consists of a steady solution plus a spectrum of standing waves whose amplitudes decay with time while their frequencies are weakly modulated owing to viscous and diffusive effects. The steady-state component of the above solution yields a withdrawal-layer thickness $O(LRa^{-\frac{1}{4}})$. The time required for this to appear is $O(N^{-1}Ra^{\frac{1}{4}}Pr^{\frac{1}{2}})$ and the above solution is valid provided $R < Pr^{-\frac{1}{2}}$. Figures 2(*a*), (*b*) and (*c*) show a typical withdrawal-layer development.

4. The convective–buoyancy withdrawal layer: $R > 1$

Let us now consider the case where convective inertia forces dominate for large times and the collapse is towards an inertial withdrawal layer of dimensional thickness $O(F^{\frac{1}{2}}L)$ which extends over the whole length of the reservoir. This occurs whenever $R > 1$, but $F^{\frac{1}{2}}L$ is smaller than the depth of the reservoir. In other words gravitational effects must be sufficient to yield a withdrawal layer and not be dominated completely by inertial forces as this would then only lead to a simple potential flow. There is no species diffusion and a quasi-steady state cannot be achieved until the fluid particles have fallen a distance equivalent to the layer thickness, that is in time $T = O(N^{-1}F^{-\frac{1}{2}})$. The corresponding density perturbation in S will be $O((d\bar{S}/dZ)LF^{\frac{1}{2}})$, so that the appropriate scaling to introduce becomes

$$x'' = XL^{-1}, \quad z'' = ZL^{-1}F^{-\frac{1}{2}}, \quad t'' = TNF^{\frac{1}{2}}, \quad s'' = S(d\bar{S}/dZ)^{-1}L^{-1}F^{-\frac{1}{2}}.$$

Introducing these new variables into (3) and (4) and dropping the primes yields

$$\psi_{zzt} + \psi_z\psi_{zzx} - \psi_x\psi_{zzz} - s_x = R^{-\frac{3}{2}}\psi_{zzzz}, \tag{20}$$

and

$$s_t + \psi_x - \psi_x s_z + \psi_z s_x = R^{-1}Pr^{-\frac{1}{2}}s_{zz}. \tag{21}$$

Some consequences of the existence of a rear wall are now obvious. In the horizontal-duct model the blocking effect due to the stratification made itself felt by the presence of a Froude number in the equations, which if too small yielded solutions with slip lines at the boundary of the withdrawal layer (see Kao 1970). This difficulty has been completely eliminated here because the behaviour specified for large Z is independent of the Froude number and is also valid for all time.

Once again the solutions of (20) and (21) will exhibit standing waves, but now their nonlinear interaction must be taken into account as well as viscous damping. However, the solution will still exhibit a discontinuity. This is most easily seen by considering the dividing streamline separating the fluid moving from above into the sink and the fluid below, which is essentially stagnant. As seen above, in times $O(L^2F^{\frac{1}{2}}/Q)$, a density difference will have formed across this dividing streamline $O((d\bar{S}/dZ)F^{\frac{1}{2}}L)$ and this difference increases with time causing the dividing streamline to possess smaller curvatures than the streamlines in the flowing layer itself. In the limit of large time it will become horizontal. However, this argument clearly shows that no steady-state solution is possible even in the absence of standing waves because the dividing streamline must attach itself to the rear wall. A stagnation point or even a tangential attachment, as discussed by Kao (1970), is not possible since both would lead to unsteady internal flows. Thus there must be a continual adjustment of the separation streamline, which in a real fluid would be masked by a viscous diffusive sublayer of thickness $O(Gr^{-\frac{1}{4}}L)$ across it.

An approximation to the outer parts of the layer, which may be expected to be immune to these minor adjustments and thus steady, may be obtained by using what is essentially an Oseen approximation of the flow variables and by replacing the dividing streamline by a zero vertical flux condition at $z = 0$. This approximation technique is only valid for long times and at the edge of the withdrawal layer, so that no attempt is made to solve the linear equation containing the unsteady terms. This question is taken up in detail in § 7, where numerical solutions are discussed. Thus let

$$\psi = x - \tfrac{1}{2} + \phi, \tag{22}$$

$$s = -t + s'. \tag{23}$$

Neglecting squared terms leads to the equation for the steady flow

$$\phi_{zzzz} - \phi_{xx} = 0. \tag{24}$$

Two more boundary conditions are required to find the solution of (24). These will be assumed to be that the pressure and density are independent of x at the free surface $z = \alpha = \lambda F^{-\frac{1}{2}}$,

$$\phi_{xx} = \phi_{zzz} = 0.$$

With these conditions the solution of (24) may be written as

$$\phi = \sum_{n=1}^{\infty} \frac{2}{n\pi} \frac{\sinh{(n\pi)^{\frac{1}{2}}(\alpha - Z)} + \sin{(n\pi)^{\frac{1}{2}}(\alpha - Z)}}{\sinh{(n\pi)^{\frac{1}{2}}\alpha} + \sin{(n\pi)^{\frac{1}{2}}\alpha}} \sin kx. \tag{25}$$

5. Flow development for fluids with a large Pr number

The above solutions are valid for Prandtl numbers $O(1)$ and cover the case of water stratified by temperature differences. Further clarification is required when $Pr \gg 1$ such as is the case for most laboratory experiments which use salt as a stratifying agent. When $R > 1$, (20) and (21) remain unaltered, indicating that the solution given by (25) remains valid. However, when $R < 1$, $Pr \gg 1$ and $Gr \gg 1$, (15) reduces to the simple form

$$\psi_{zztt} - \psi_{zzzzt} + \psi_{xx} = 0. \tag{26}$$

This equation describes the evolution of shear waves into a withdrawal-layer structure at $t = O(1)$. For $t > 1$, this equation admits an approximate self-similar solution of the form

$$\psi = \psi(zt^{\frac{1}{4}}/x^{\frac{1}{2}}), \tag{27}$$

indicating that the layer experiences a further collapse with time, and it is not difficult to show that in the limit $t \to \infty$ the solution to (26), satisfying the appropriate boundary conditions, becomes $\psi = \frac{1}{2}x + \frac{1}{2}(x-1)\operatorname{sgn} z$. Substitution of (27) into (15) shows that the self-similar solution is a valid approximation until either species convection or diffusion has grown to the same magnitude as the convection of the background density gradient.

If $R < Pr^{-\frac{1}{6}}$ then diffusion is the first to grow to $O(1)$ and after times

$$O(N^{-1}Gr^{\frac{1}{4}}Pr^{\frac{2}{3}})$$

this term must be accounted for. It is not difficult to show that for this case the equations are identical to the pseudo-steady state described in § 3. Associated with this pseudo-steady flow is a density perturbation

$$\varphi = (-\psi_x + \psi_{xx})t. \tag{28}$$

This variation leads to the gradual formation, at the level of the sink, of a horizontal step structure in the density field. The density jumps across this layer will be $O((d\bar{S}/dZ)\,QTL^{-1})$ and the thickness will be $O(Ra^{*-\frac{1}{4}}L)$, where Ra^* is the Rayleigh number based on the gradient across this layer. For times

$$O(N^{-1}Gr^{\frac{1}{4}}Pr^{-\frac{1}{6}}R^{-1})$$

this perturbation will become of the same order as the background stratification and Ra^* will become appreciably different from Ra. If one notes that $R \to 0$ as $d\bar{S}/dZ \to \infty$, it is not difficult to show that for such large times $s_x = 0$ to first order; to second order the equations are the same as the above. This leads to a withdrawal-layer structure which is essentially the same as that described by (17), but which slowly evolves in time yielding a withdrawal-layer thickness

$$\delta = O(LRa^{-\frac{1}{4}}Pr^{-\frac{1}{6}}R^{-\frac{1}{6}}t^{-\frac{1}{6}}), \quad \text{where} \quad t = T/N^{-1}Ra^{\frac{1}{4}}Pr^{\frac{1}{2}}.$$

On the other hand if $Pr^{-\frac{1}{6}} < R < 1$ the collapse is first modified by the convection terms which accelerate the collapse process. Steady state is essentially analogous to the solution given by Imberger (1972) and is dominated by viscous effects if $Pr^{-\frac{1}{6}} < R < Pr^{-\frac{1}{3}}$ and inertial effects if $Pr^{-\frac{1}{3}} < R < 1$. It was shown by

Imberger (1972) that for a fluid with $Pr = O(1)$ the inertial zone extends out a distance $O(R^{\frac{3}{2}})$. For large Prandtl number this distance must be modified to $R^{\frac{3}{2}}Pr^{\frac{1}{4}}$ where species convection begins and $R^{\frac{3}{2}}$ where inertia forces begin. This explains why the numerical solution for large Prandtl number found by Imberger (1972) did not approach the linear solution until x/x_c was quite large. No analytic solution could be found for these complex phenomena and the authors resorted to a numerical solution of the complete equations to obtain further insight. A summary of all the time and length scales possible is given in table 1.

6. Numerical solution

An Eulerian finite-difference method is not appropriate for the above flows where large density differences develop (see Thompson 1976). Lagrangian grids are also unsuitable since these would become too distorted within the withdrawal-layer structure. The particle-in-cell method of Harlow & Welch (1965) and the cloud-in-cell method of Birdsall & Fuss (1969) seem to combine the best features of both Eulerian and Lagrangian approaches, so it was decided to adapt these methods for a stratified, incompressible fluid.

If the ζ is the vorticity and ρ the total density, then (3) and (4) may be written

$$D\zeta/Dt = -(g/S_0)\,\partial\rho/\partial x + \nu\nabla^2\zeta, \tag{29}$$

$$D\rho/Dt = \kappa\nabla^2\rho. \tag{30}$$

The fields ζ and ρ are described by a cloud of n particles each labelled with X_k, Z_k, ζ_k, ρ_k and a parameter C_k, called ink. This last parameter is a convenient label for tracing the particles' motion. Given the field ζ, one may obtain the velocities from the solution of the equation

$$\nabla^2\Psi = \zeta, \tag{31}$$

and the boundary conditions (6). This velocity is then used to move the particles to their new positions. The labels of each particle are adjusted using (29) and (30). These are linear operations, so that an Eulerian grid is the most suitable.

The essential part of the particle-in-cell method is the connexion between the Lagrangian particles and the Eulerian fields. This is done by interpolation, the price for handling both advection and diffusion correctly. The Eulerian field for vorticity is called Z_{ij} and X is regarded as being at a fixed position $((i-1)\Delta X$, $(j-1)\Delta Z)$ and the density R_{ij} at $((i-\frac{1}{2})\Delta X$, $(j-\frac{1}{2})\Delta Z)$. It is easy to find which grid point a given particle is closest to:

$$i = (X_k/\Delta X) + \tfrac{1}{2}, \quad j = (Z_k/\Delta Z) + \tfrac{1}{2}, \tag{32}$$

but there is no way to find which particles are near to a given grid point, other than by searching the entire list. [This searching is really what makes Lagrangian methods impractical.] Therefore, the program must proceed through the list of particles, finding the closest points to each, adding the sums for Z, R, and the number of particles at each grid point. In order to simulate correctly internal gravity waves which have the property that small displacements cause small, continuous changes, particles will not be thought of as being point-like, but

rather as small volumes requiring the use of bilinear interpolation. This is equivalent to regarding each particle as being of size $\Delta X \times \Delta Z$, and weighting the allocation of ζ_k to Z_{ij} (and ρ_k to R_{ij}) by the overlap of area with the $\Delta X \times \Delta Z$ cell centred at Z_{ij} (or R_{ij}). Thus, as a particle moves up into a cell, its density ρ_k will have a continuously increasing influence on R_{ij}. This approach is similar to the 'clouds' used by Birdsall & Fuss (1969). After the new R and Z fields are found by this averaging, finite differences are used to compute DR/Dt and DZ/Dt; these are linearly interpolated back to each particle (again running through the lists). The stream function ψ is found by relaxing $\nabla^2\psi = Z$, and the velocities U and V are found by finite differencing. The particles are moved by the linearly interpolated velocities, and now the new R and Z can be found.

7. Results from numerical experiments

Evolution to a withdrawal layer

Figure 3 shows the time development of the flow in a square tank for the particular case in which $Pr = 7{\cdot}07$ and $R = 0{\cdot}043$, so that $R < Pr^{-\frac{1}{3}}$ and the evolution will be towards a layer of thickness $O(LGr^{-\frac{1}{3}})$ in a time $O(N^{-1}Gr^{\frac{1}{3}})$, with secondary collapse to a layer $O(LRa^{-\frac{1}{3}})$ in times $O(N^{-1}Ra^{\frac{1}{3}}Pr^{\frac{1}{2}})$. It is seen from figure 3 that the potential flow, which exists soon after the initiation of the sink, is replaced by a flow consisting of a series of shear waves travelling backwards and forwards across the tank which after a short time expand to become standing waves. Inspection of the vertical velocity indicates that the first and second modes have become standing waves when $TN\lambda^3 = 0{\cdot}6$ and $TN\lambda^3 = 1{\cdot}2$ respectively. The non-dimensional time for complete decay is equal to $O(Gr^{\frac{1}{3}}\lambda^2)$, which has the value of 134·52, so that the first mode will oscillate long after the withdrawal layer has formed. This is illustrated in figure 3 (*d*), which shows that the final withdrawal layer has essentially already formed for $t' = 1{\cdot}1$, but as seen from the velocity plots of figure 5(*a*) the upper fluid continues to oscillate. The computations were terminated at $t' = 1{\cdot}44$ because of computing costs. Figure 4 is a plot of withdrawal-layer half-thickness (where $u/u_0 = 0{\cdot}5$) at the centre of the box against non-dimensional time t'. From this it is seen that the withdrawal-layer thickness rapidly thins as $Gr^{-\frac{1}{12}}(NT)^{-\frac{3}{4}}$ while the shear waves progressively arrive, until $t' = 1$ when the thinning slows and the secondary collapse commences. In the present case this should be completed when $t' = 3{\cdot}67$ when the dimensionless thickness will be of order $Pr^{-\frac{1}{3}} = 0{\cdot}7$. The secondary collapse is more apparent for larger Pr numbers and figure 4 also shows data from $Pr = 16{\cdot}54$, 915 and $3{\cdot}5 \times 10^5$ and ∞. The last three examples illustrate the secondary collapse extremely well, but computational time was too great for the secondary layer to form. The intermediate example of a $Pr = 16{\cdot}54$ shows clearly the secondary layer forming and the time to reach steady state is very close to the scaling estimate. All the values of the relevant dimensionless groups are shown in the figure caption.

The horizontal velocity profiles shown in figure 5(*b*) show the approach to steady state for the case $R = 4{\cdot}3$, $Pr = 7{\cdot}07$ and figure 6 depicts the streamlines at $t'' = 2{\cdot}2$, clearly showing the approach to the Oseen approximation derived in

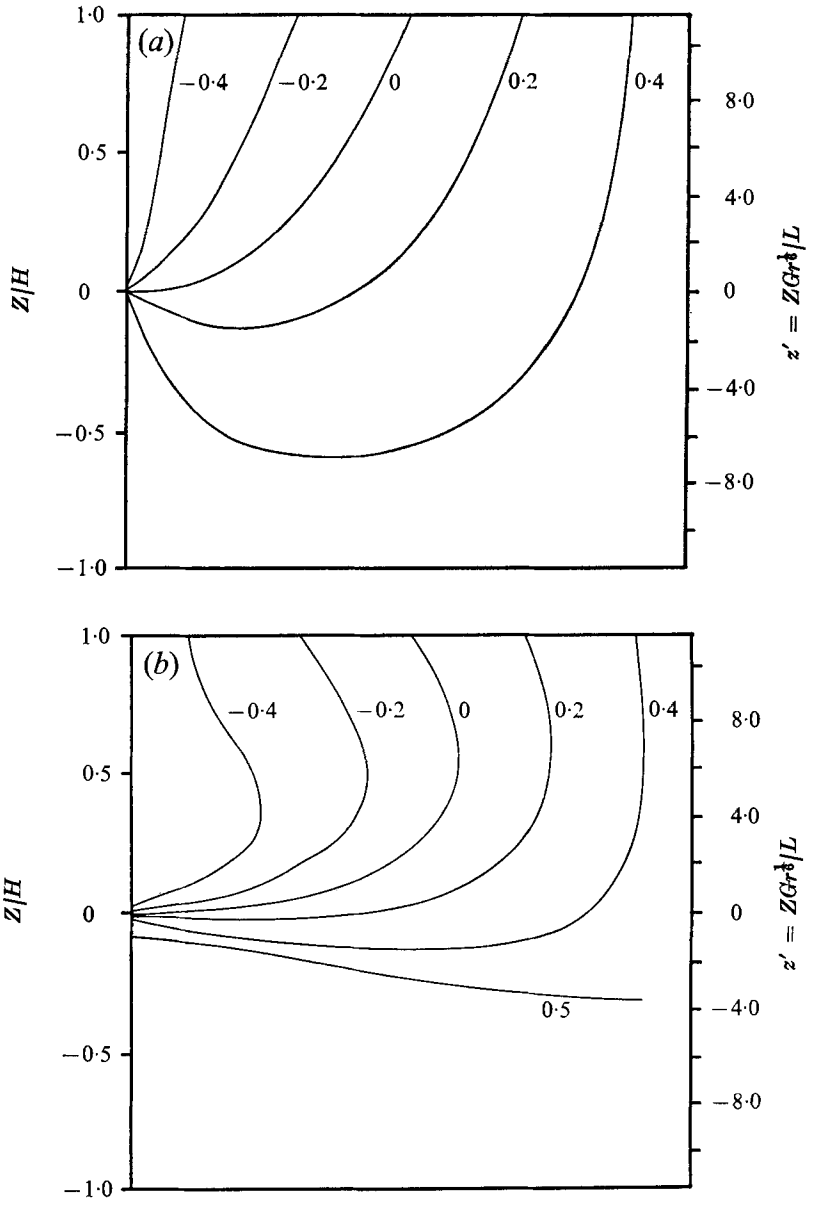

FIGURES 3(*a*) and (*b*). For legend see p. 502.

§3 (dashed line). The oscillations are more severe in this case and take somewhat longer to decay. As a final example both ν and κ were set to zero. The solution showed the formation of a steady withdrawal layer at $t'' \approx 0{\cdot}6$, but sloshing continued to the end of the run at $t'' = 1{\cdot}6$, indicating that with no viscosity present the larger internal waves will remain indefinitely. This sloshing became less severe when λ was decreased to 0·20.

To check the dependence on the aspect ratio and to allow a comparison with the solutions derived in the previous sections, we ran $\lambda = 0{\cdot}1$ for $R = 1{\cdot}77$ and

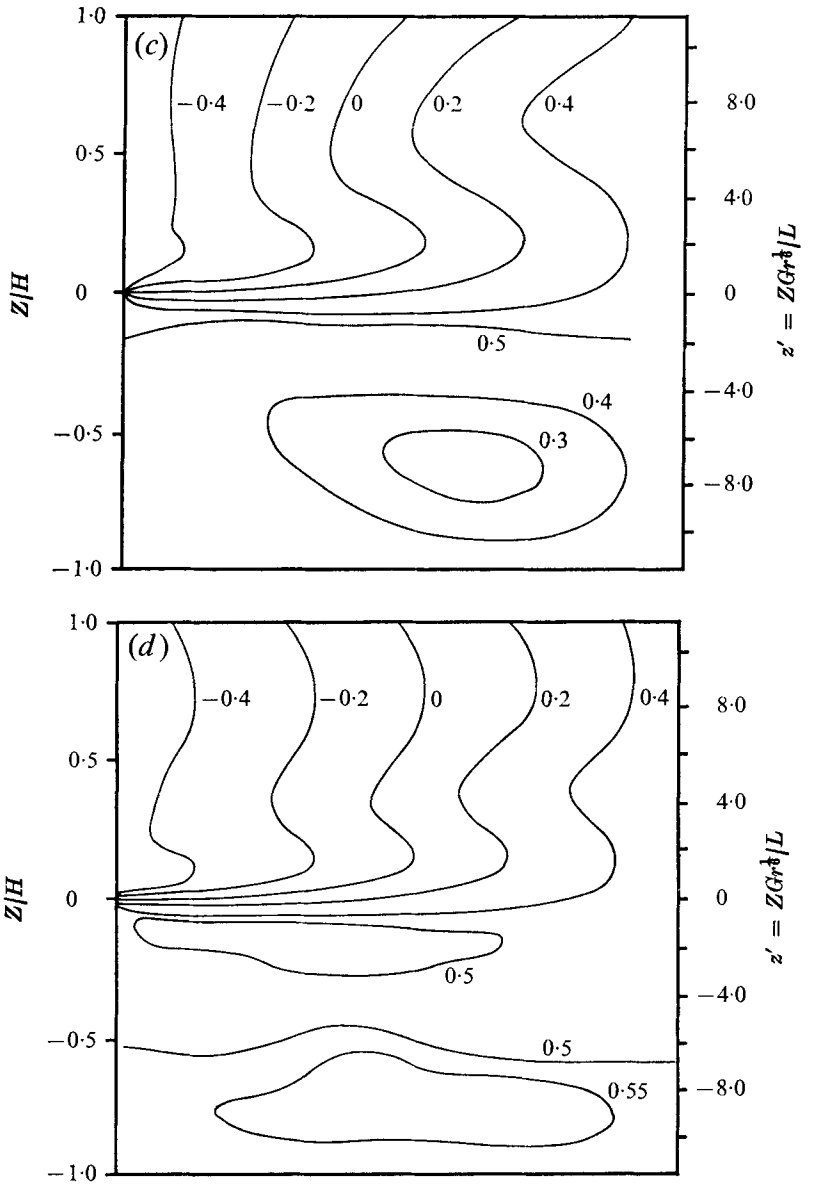

FIGURE 3. Streamlines for withdrawal from a thermally stratified reservoir with $R < 1$, from the numerical algorithm. Parameters are $F = 8 \times 10^{-5}$, $Gr = 1{\cdot}56 \times 10^{8}$, $Pr = 7{\cdot}045$, $R = 0{\cdot}043$, $\lambda = 0{\cdot}5$. (*a*) $t' = 0{\cdot}0$. (*b*) $t' = 0{\cdot}216$. (*c*) $t' = 0{\cdot}647$. (*d*) $t' = 1{\cdot}078$.

$Pr = 7{\cdot}045$. Comparison of the theory with the present case and the above square-box examples showed that the solution within the layer became independent of λ after $t'' \approx 0{\cdot}08$; before this time smaller aspect ratios exhibited a rather more radial type of flow near the origin. The wave motion, or rather the number of waves present, when the wave with the layer wavenumber has reached the end wall, i.e. $t'' = 1$, depends of course critically on λ. The larger the value of λ

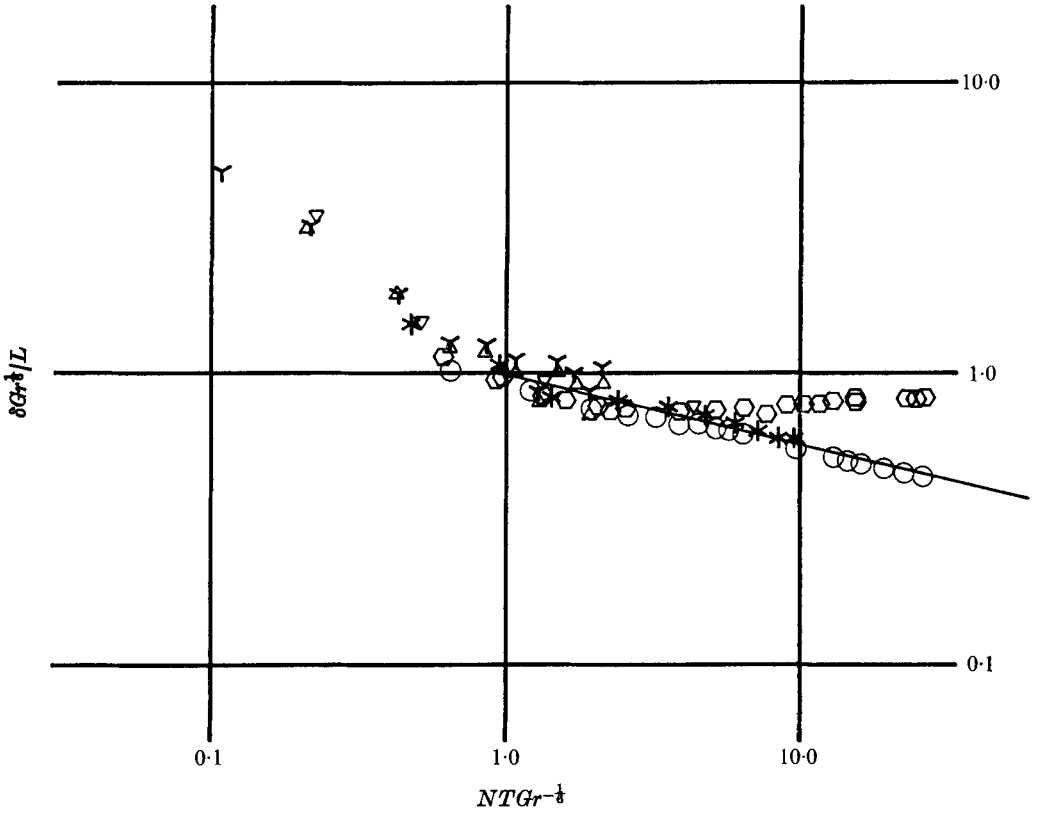

FIGURE 4. Withdrawal-layer thickness, at $X/L = 0{\cdot}5$, versus time. The layer thickness δ is defined as the distance from $Z = 0$ to the point where the velocity has decreased to half the maximum value. The straight line has a slope $-\frac{1}{4}$.

Symbol	F	Gr	R	Pr	Steady-state formation $N^{-1}Gr^{\frac{1}{6}}$	Characteristic layer thickness $LGr^{-\frac{1}{6}}$	Regime
Y	$8{\cdot}0\times10^{-3}$	$1{\cdot}6\times10^{8}$	$4{\cdot}3\times10^{-2}$	7·07	3·7	$7{\cdot}2\times10^{-1}$	*a*
o	$8{\cdot}0\times10^{-4}$	$3{\cdot}2\times10^{3}$	$1{\cdot}2\times10^{-4}$	$1{\cdot}61\times10^{1}$	6·5	$6{\cdot}3\times10^{-1}$	*a*
*	$8{\cdot}0\times10^{-5}$	$1{\cdot}2\times10^{6}$	$8{\cdot}5\times10^{-3}$	$9{\cdot}15\times10^{2}$	$9{\cdot}4\times10^{1}$	$3{\cdot}2\times10^{-1}$	*b*
○	$8{\cdot}0\times10^{-3}$	$3{\cdot}2\times10^{3}$	$1{\cdot}8\times10^{-3}$	$3{\cdot}50\times10^{5}$	$4{\cdot}9\times10^{3}$	1·1	*b*
△	$8{\cdot}0\times10^{-5}$	$1{\cdot}6\times10^{8}$	$4{\cdot}3\times10^{-2}$	∞	∞	0	*c*
▽	$1{\cdot}1\times10^{-4}$	$1{\cdot}1\times10^{10}$	$2{\cdot}4\times10^{-1}$	$6{\cdot}96\times10^{2}$	$1{\cdot}7\times10^{1}$	$4{\cdot}9\times10^{-1}$	*c*

the more modes will traverse the tank before the layer has formed. Comparison of the number of waves present at $t'' = 1$ was always in accordance with theory ($2\lambda/\pi F^{\frac{1}{2}}$ for $R > 1$ or $2\lambda/\pi Gr^{-\frac{1}{6}}$ for $R < R^{-\frac{1}{6}}$).

Effect of a variable stratification

Most previous investigators, with the exception of Wood & Lai (1972), have dealt with the constant-N fluid. However, it is trivial to change the initial stratification in the numerical model. As an illustration, the following example, representative

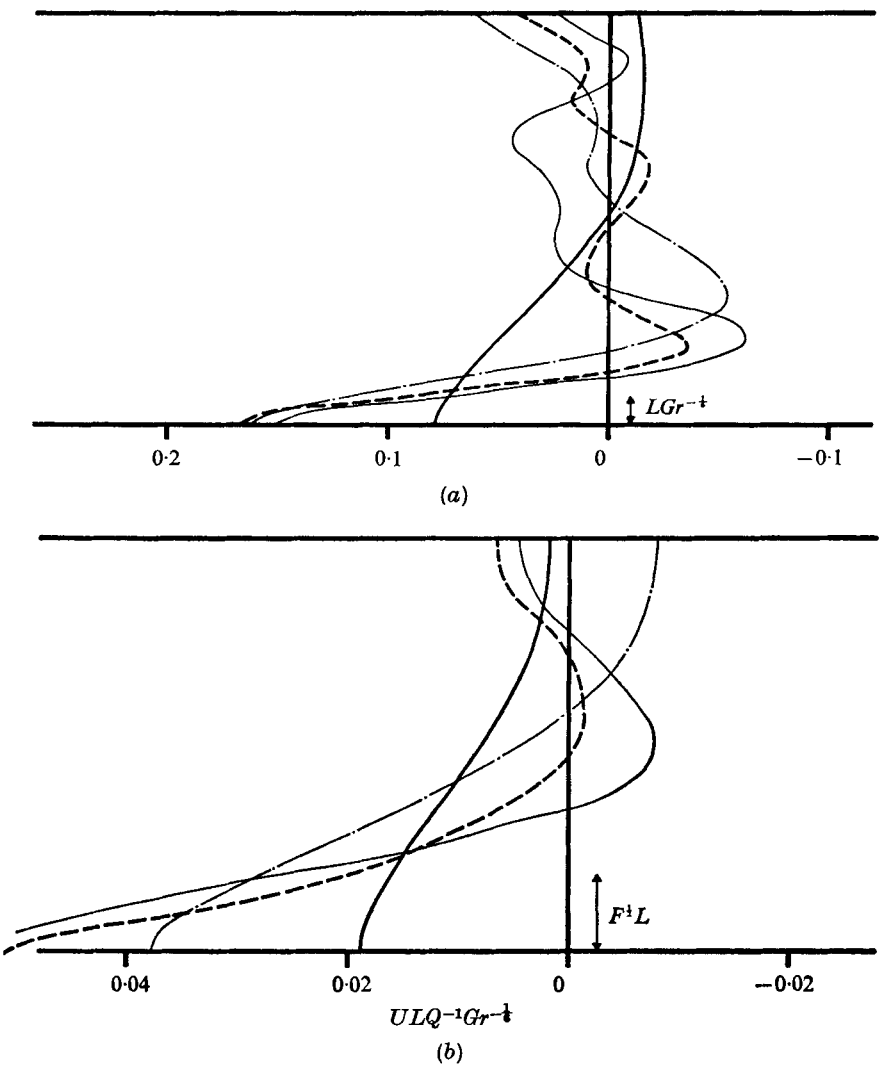

FIGURE 5. Velocity profiles at $X/L = 0{\cdot}5$ for various times. (*a*) Parameters as in figure 3 ($R < 1$). ——, $t' = 0{\cdot}16$; —·—, $t' = 0{\cdot}48$; ——, $t' = 0{\cdot}96$; – – –, $t' = 1{\cdot}44$. (*b*) Parameters as in figure 6 ($R < 1$). ——, $t' = 0{\cdot}22$; —·—, $t' = 0{\cdot}44$; ——, $t' = 0{\cdot}88$; – – –, $t' = 2{\cdot}2$.

of some reservoirs, was chosen: a well-mixed layer on the top, a fossil homogeneous layer on the bottom, and a thermocline between. This run was like previous examples in a square box with R based on the central value of N equal to 4·30. The upper and lower quarter of the tank was filled with water at N equal to zero. With the outlet in the thermocline, everything was much as before and a layer of thickness $LF^{\frac{1}{2}}$ formed. With the outlet moved to a height of 0·1 m, just below the thermocline, events were more interesting. Wood & Lai (1972) analysed a similar situation of an outlet below an interface between two constant densities. They found that, if the density difference was not too much, the upper fluid would be drawn down near the outlet. Here, the density difference starts at zero,

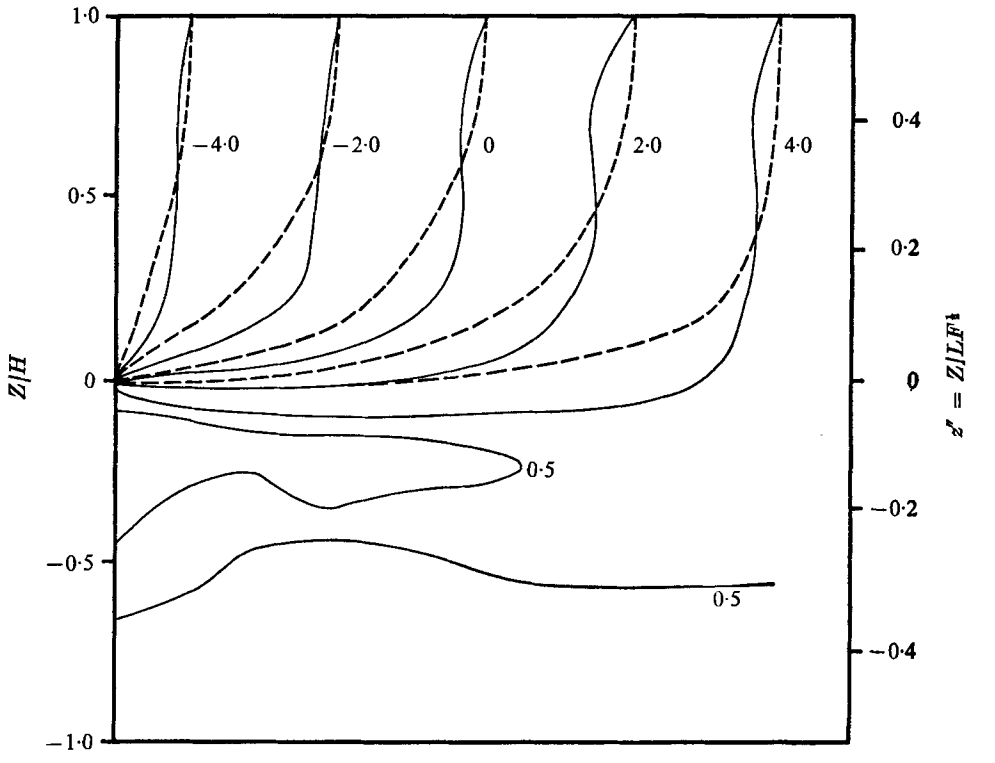

FIGURE 6. Streamlines for withdrawal from a thermally stratified reservoir with $R > 1$, from the numerical algorithm and Oseen approximation. Parameters are $F = 8 \times 10^{-3}$, $Gr = 1{\cdot}56 \times 10^{8}$, $Pr = 7{\cdot}045$, $R = 4{\cdot}30$, $\lambda = 0{\cdot}5$, $t' = 2{\cdot}203$; ——, numerical value; – – –, Oseen approximation.

so we can expect part of the thermocline ('upper layer') to be drawn down, but expect the further parts, with greater density difference and distance, to be affected less.

After the start, the flow remained close to potential flow longer than previous runs. However, at a stage in the drawing down of the thermocline, some 'resonance' was excited, for a wave with a much sharper shear front than previously observed ran down the tank and set up a much more vigorous fundamental-mode standing wave than previously seen. Despite this, the streamlines, when averaged over several wave periods, were virtually vertical through the thermocline, and did their bending as potential flow in the layer. The main effect of the outlet was to cause the entire thermocline to drop rather uniformly, without any sharp layer forming. Most of the outflow was from the lower layer until after the bottom of the thermocline fell below the outlet. After this, the vertical convergence of the thermocline stratification formed a conventional $F^{\frac{1}{4}}L$ layer.

From this example, we can speculate about the effects of general variable stratification. The inertial- and viscous-layer thicknesses are proportional to $N^{-\frac{1}{2}}$ and $N^{-\frac{1}{3}}$, so if the stratification decreases, the layer thickness should increase (though not a lot). Therefore, if the outlet is in vertically varying N, the side with lower N should have the wider layer. With roughly equally spaced streamlines,

the greater flow can be expected from that side. The streamlines will tend to avoid the stronger stratification, causing more convergence in the weaker stratification.

Inflow

The inflow of a homogeneous fluid into a stratified tank may now be treated similarly. Attention is confined here to cases where the entering fluid has the same density as the fluid adjacent to the opening and also where the inflow momentum is small (wide openings). Hydraulic jumps and entraining plunging flows are beyond the scope of laminar flow theory.

When the inflow is neutrally buoyant, exact symmetry exists between the scaling of the outflow problem and the inflow problem. The chief difference will be the occurrence of a slug of nearly homogeneous water emerging from the source. The equations of motion, for the initial state, and the boundary conditions are all the same as before, except that the sign on the stream function was reversed. For outflow, it was found that the behaviour of the withdrawal layer was controlled by the ratio of the inertial to viscous forces given by $R = FGr^{\frac{1}{4}}$ and secondarily by the Prandtl number. The following regimes are once again distinguishable.

(i) $R > 1$. The flow is dominated by a balance of inertial and buoyancy forces. From the discussion for outflow, we expect a layer thickness $O(F^{\frac{1}{2}}L)$, and a length $LTNF^{\frac{1}{2}}$. Thus the slug will penetrate the length of the tank in an inertial set-up time $O(N^{-1}F^{-\frac{1}{2}})$. However, the inertial set-up time was the time for outflow to cause the fluid to fall a distance $O(F^{\frac{1}{2}}L)$; for flow-in, the fluid will rise the same distance in the same time. Furthermore, the flow near the slug may be expected to act as though set up even before the 'set-up time' for the whole tank, as the slug has already forced the stratified fluid apart locally. Manins (1976) also proposed this slug thickness and length, using very different reasoning. The equations governing the flow are thus identical to those governing the inertial outflow problems [(20) and (21)].

Figure 7 shows a typical streamline pattern obtained from the numerical algorithm for $R = 5{\cdot}95$ and $Pr = 7{\cdot}07$. A wide entrance was used ($\frac{1}{5}$ of the depth) to avoid a high momentum input. The slug can be seen to narrow quickly to the width of $2{\cdot}4F^{\frac{1}{2}}L$ and rise gently as it moves out. Both phenomena were also observed by Manins (1976) in his physical experiments. Comparison of this numerical run and Manins (1976) data is shown in table 2, where $C = X/LTNF^{\frac{1}{2}}$ is tabulated for the different runs. Good agreement may be noted, but, as already pointed out by Manins (1976), the propagation speed is influenced by the shear waves leaving the slug region as these travel at approximately the same speed as the slug itself.

(ii) $Pr^{-\frac{1}{6}} < R < 1$. The initiation of the source causes shear waves to move out ahead of the slug of entering fluid and set up an inertial layer close to the source (up to a distance $O(LR^{\frac{3}{2}})$) and a forward viscous wake of thickness $O(LGr^{-\frac{1}{4}})$ beyond this. The flow field in front of the slug will become viscous after times $O(N^{-1}Gr^{\frac{1}{4}}R)$ while the whole forward layer takes $O(N^{-1}Gr^{\frac{1}{4}})$ to form. As soon as the viscous layer has formed it begins to collapse, as described in § 5, intensifying the density gradient in front of the moving slug. This process, however, occurs on

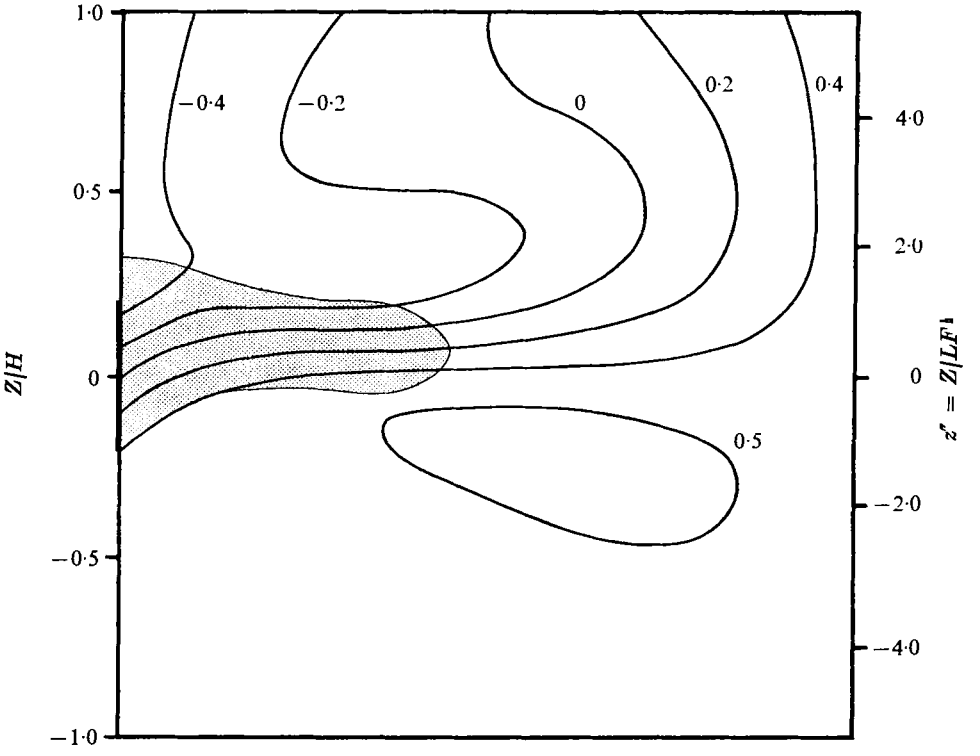

FIGURE 7. Inflow into a thermally stratified fluid showing streamlines and slug position. Parameters are $F = 8 \times 10^{-3}$, $Gr = 1{\cdot}56 \times 10^{8}$, $Pr = 7{\cdot}07$, $R = 4{\cdot}30$, $\lambda = 0{\cdot}5$, $t' = 0{\cdot}894$.

a very much longer time scale than $N^{-1}Gr^{\frac{1}{3}}$ and thus the solution in the forward wake will be closely approximated by the similarity solution (27). This, therefore, leads to a slug displacement $l = CLR^{\frac{2}{3}}(t')^{\frac{5}{3}}$ causing a compression of the fluid in front of the slug which counteracts the previously mentioned collapse. The motion is thus self-similar and the $T^{\frac{5}{3}}$ behaviour may be expected to hold until the slug is very close to the end wall. The slug reaches the end wall in times $O(N^{-1}Gr^{\frac{1}{3}}R^{-\frac{1}{3}})$, which is exactly the time required in the outflow problem for convection to become appreciable. Hence once again the scaling shows exact symmetry with the outflow problem. Thus if $R > Pr^{-\frac{1}{3}}$ the slug reaches the end before the forward wake has collapsed appreciably. All of Maxworthy's (1972) experiments and most of those of Zuluaga-Angel, Darden & Fischer (1972) fall into this regime, and table 2 lists the values of C and the exponents of T for the non-entraining runs.

The runs with large entrainment (carried out by both investigators) generally move faster than predicted and follow a $T^{\frac{3}{4}}$ law. This may be explained by noting that the entrainment on either side of the source induces large backflows (see also Darden, Imberger & Fischer 1972), which in turn induce forward flow at the level of the source. No attempt is made here, however, to describe the jump characteristics.

(iii) $R < Pr^{-\frac{5}{6}}$. The initiation of the sink leads to a flow essentially identical to

Investigator	Experiment number	Pr	R	T/N^{-1} $Gr^{\frac{1}{3}}R$ at start	T/N^{-1} $Gr^{\frac{1}{3}}R$ at finish	C	Average C	Exponent	Average exponent
Zuluaga-Angel *et al.*	Run 11	796	0·099	0·39	185·0	0·443	0·460	0·81	0·79
	Run 12	811	0·077	4·67	265·5	0·477		0·76	
Maxworthy	Q = 6·1	811	0·0226	8·97	173·6	0·460	0·522	0·82	0·81
	Q = 12	811	0·0445	5·1	53·2	0·554		0·81	
	Q = 64	811	0·237	0·43	6·9	0·520		0·82	
	Q = 130	811	0·482	0·21	2·3	0·535		0·80	
Manins	A	811	0·403	0·80	3·6	0·342	0·405	0·89	1·10
	F	811	3·670	0·05	0·2	0·342		1·32	
	J	811	0·799	0·10	0·4	0·468		1·14	
	M	811	2·410	0·03	0·4	0·468		1·06	
Numerical	Heat	7·07	4·303	0·04	0·14	0·470	0·470	1·04	1·04
Algorithm	Salt	9·09	4·303	0·04	0·14	0·461	0·461	1·06	1·06

TABLE 2

that just described in (ii). However, now the forward wake collapses to a viscous diffusive layer in time $O(N^{-1}Gr^{\frac{1}{3}}RPr^{\frac{2}{3}})$, before the slug reaches the end. From this point on, the readjustment of the wake caused by the entering layer occurs on time scales $O(N^{-1}Gr^{\frac{1}{3}}Pr^{\frac{2}{3}})$, which is much smaller than the time required for the slug to traverse the tank, which is $O(N^{-1}Gr^{\frac{1}{3}}Pr^{-\frac{1}{3}}R^{-1})$, the time required for convection to modify the gradient! Thus the motion of the slug may be described by a pseudo-steady flow being slowly modulated with time. The relation $l = CLR^{\frac{3}{4}}Pr^{\frac{1}{3}}(t')^{\frac{1}{4}}$ is thus valid in this regime.

In summary, the inflow slug speed may in general be described by

$$l' = l/LR^{\frac{3}{4}} = f(T/N^{-1}Gr^{\frac{1}{3}}R; Pr) = f(t'/R; Pr). \tag{33}$$

For $t' \leqslant R$ the flow is inertial and described by

$$l' = Ct'/R, \tag{34}$$

where, from table 2, C may be taken as 0·44. For $R < t' < Pr^{\frac{2}{3}} < R^{-\frac{1}{3}}$ viscosity dominates the flow and we have

$$l' = C(t'/R)^{\frac{1}{3}}, \tag{35}$$

where $C = 0{\cdot}491$. For $Pr^{\frac{2}{3}} < t' < R^{-1}$ viscosity and diffusion dominate the flow and

$$l' = C(t'/R)^{\frac{1}{4}}Pr^{\frac{1}{3}}. \tag{36}$$

Unfortunately no data exists for this regime and none could be generated numerically owing to the large computing times associated with such slow flows.

8. Comparison with field and laboratory data

Consider first laboratory data. The evolution of the shear waves into a withdrawal structure for flows where $R \gg 1$ has recently been studied by Kao *et al.* (1975). They considered only the region very near the sink ($X/L < 0{\cdot}08$) where steady state was achieved before reflexions from the end wall returned to the field of view. Comparison of their work with figure 6 shows that provided X/L is small and R large the evolution and steady state are independent of the value of R and the model chosen.

Experiments in which $Pr^{-\frac{1}{3}} < R < 1$ have recently been carried out by Silvester (1977) and attention will be concentrated on a salt stratification example where $R > Pr^{-\frac{1}{3}}$ and where the time scales are separated as much as possible. Figure 8 shows a typical streamline pattern obtained by averaging particle paths over 10 s. The dashed lines are the averages of numerically computed streamlines for the same set of parameters. The layer collapse is plotted in figure 4 and once again the secondary collapse is observed. In the experiment the longer waves did remain, sloshing the fluid back and forth, but their decay was not measured. Agreement with the numerical results was good in all cases.

Comparison with field data is most difficult because reservoirs are generally irregular and because the river bed has a gently slope, so that the container is shaped more like a triangular vessel than a rectangular tank. However, if L is

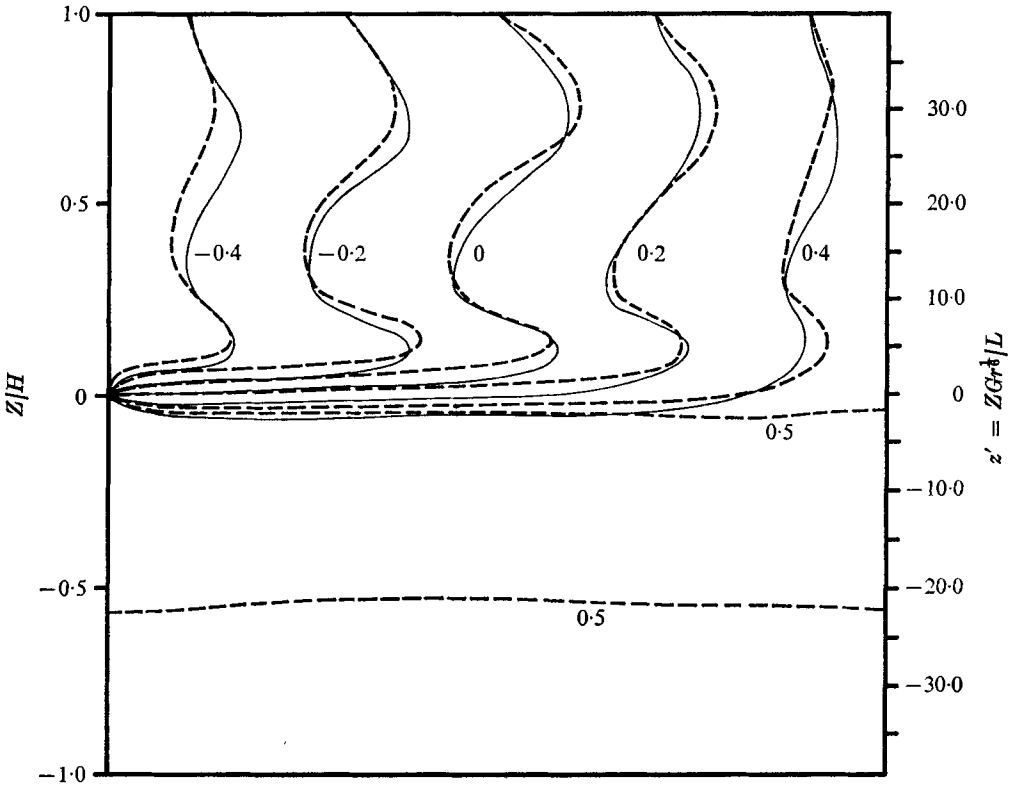

FIGURE 8. Average streamline pattern for withdrawal from a salt stratified tank. Parameters are $F = 1{\cdot}11 \times 10^{-4}$, $Gr = 1{\cdot}06 \times 10^{10}$, $Pr = 697$, $R = 0{\cdot}243$, $\lambda = 0{\cdot}5$, $t' = 0{\cdot}232$–$0{\cdot}311$; ——, experimental value from Silvester (1976); – – –, numerically computed values.

taken as the length from the outlet to where the river bed reaches the same elevation as the outlet, very good agreement can be achieved without the necessity of postulating large eddy exchange coefficients. Two sets of field data exist. First, there are the T.V.A. data where $R \gg 1$ and where velocities and withdrawal-layer thicknesses were measured directly, and, second, there are the data presented by Imberger (unpublished) where velocities are deduced from the movement of naturally occurring salt concentrations. Table 3 shows the available data with the predictions obtained from the numerical results by matching Pr and R. All calculations are based on molecular exchange coefficients with the fluid contained in a square box. No attempt was made to compare the wave motion with the field data since Kao *et al.* (1974) have already verified times of arrival of the first few shear waves.

A major discrepancy arose in the induced velocities near the rear of the reservoir where the withdrawal layer impinges on the gently sloping river bed. However, if one remembers that, in surface area, a major part of the reservoir may lie behind the observation point it is not surprising that the induced velocities are much higher than predicted, and a horizontal duct model would be more appropriate for predicting the induced velocities. Inspection of table 3 shows that

Name of reservoir ...	Cherokee	Cherokee	Cherokee	Cherokee	Fontana	Wellington	Wellington
Date ...	17. 8. 67	20. 9. 67	16. 8. 67	14. 9. 67	9. 9. 66	31. 10. 74	22. 12. 74
Basic Parameters							
N (s^{-1})	0	0·0105	0·0194	0·0230	0·0190	0·022	0·028
L (m)	16500	16500	16500	16500	14500	16000	16000
$\nu \times 10^6$ ($m^2\ s^{-1}$)	0·984	1·01	1·01	1·01	1·01	1·10x	1·10
$\kappa \times 10^7$ ($m^2\ s^{-1}$)	1·41	1·41	1·41	1·41	1·41	1·41x	1·41
Q ($m^2\ s^{-1}$)	0·520	0·483	0·624	0·353	0·706	0·0134	0·0068
$T \times 10^{-5}$ (s)	0·43	0·43	0·43	0·43	0·43	103·6	45·8
X (m)	640	640	2739	15500	1046	4600	4600
Computed parameters							
Pr	6·98	7·17	7·16	7·16	7·16	7·86	7·86
$Gr \times 10^{-25}$	2·24	0·62	2·13	2·99	1·56	2·62	4·25
$F \times 10^9$	111·6	191·5	133·8	63·9	176·7	2·38	9·43
R	31·5	35·2	37·1	19·9	44·2	0·709	0·329
t''	0·279	0·196	0·305	0·250	0·34	—	—
t'	—	—	—	—	—	13·2	6·73
Flow regime	$R \gg 1$	$R \gg 1$	$R \gg 1$	$R \gg 1$	$R \gg 1$	$Pr^{-\frac{1}{3}} < R < 1$	$Pr^{-\frac{1}{3}} < R < Pr^{-\frac{5}{6}}$
Predicted total layer thickness (m)	18·0	23·2	24·4	Full depth 36·6 m (15·7) steady state	22·7	4·1	2·9
Observed total layer thickness (m)	22·9	24·4	25·9	21·3	27·4	6	5
Predicted peak velocities ($m\ s^{-1}$) (Horizontal duct model)	0·039	0·022	0·052	(0·044)	0·030	0·00093†	
Observed peak velocities ($m\ s^{-1}$)	0·046	0·039	0·053	0·030	0·027	0·00077†	
Primary time of layer formation ($N^{-1}Gr^{\frac{1}{6}}$) (days)	—	—	—	—	—	9·07	7·72
Final time of layer formation in (days)	1·79	2·52	1·63	1·99	1·45	15·6	30·5

TABLE 3. Comparison with field data. † Displacement measured over the period 31. 10. 74 to 22. 12. 74. ‡ From a run of same R and Pr with in- and outflow.

the predictions are generally excellent and there is little need to invoke turbulent mixing on days when the stratification is stable with $R > 1$ and only nominal increases when $R < 1$. Furthermore, the layer thickness are reasonably independent of the end boundary condition, whether open or closed, since the layer is set up from the sink. However, the length L is critical in determining the time scales of collapse. The reflexion of waves and the possible evolution into standing waves would naturally be complicated by the sloping bottom, but no data exists for this at present.

REFERENCES

BIRDSALL, CHARLES, K. & FUSS, D. 1969 *J. Comp. Phys.* **3**, 494–510.

DARDEN, B. R., IMBERGER, J. & FISCHER, H. B. 1972 *A.S.C.E. J. Hydraul. Div.* **101**, 1211–1220.

GELHAR, L. W. & MASCOLO, D. M. 1966 *M.I.T. Hydraul. Lab. Rep.* no. IV 088, pp. 1–39.

HARLOW, F. H. & WELSH, J. E. 1965 *Phys. Fluids*, **8**, 2182–2183.

KAO, W. T. 1970 *Phys. Fluids*, **13**, 535–543.

KAO, W. T., PAO, H. P. & WEI, S. N. 1974 *J. Fluid Mech.* **65**, 689–710.

JANOWITZ, G. S. 1968 *J. Fluid Mech.* **33**, 417–432.

IMBERGER, J. 1972 *J. Fluid Mech.* **53**, 329–349.

IMBERGER, J. & FANDRY, C. B. 1975 *J. Fluid Mech.* **70**, 321–332.

MCEWAN, A. D. & BAINES, P. G. 1974 *J. Fluid Mech.* **63**, 257–272.

MANINS, P. C. 1976 *J. Fluid Mech.* **74**, 547–560.

MAXWORTHY, T. 1972 *IAHR/AIRH Int. Symp. Stratified Flows, Novosibirsk*, paper 17.

PAO, H. P. & KAO, W. T. 1974 *J. Fluid Mech.* **65**, 657–688.

SILVESTER, R. 1977 Ph.D. thesis, University of Western Australia.

THOMPSON, R. O. R. Y. 1976 *J. Fluids & Comp.* (in Press).

WOOD, I. R. & LAI, K. K. 1972 *J. Hydraul Res.* **10**, 475–496.

ZULUAGA-ANGEL, A., DARDEN, R. B. & FISCHER, H. B. 1972 *U.S. Environ. Protection Agency Rep.* no. R2-72-037. Washington D.C.